Production of charged Higgs bosons of the minimal supersymmetric standard model in b-quark-initiated processes at the CERN Large Hadron Collider

Stefano Moretti

Cavendish Laboratory, University of Cambridge, Madingley Road, Cambridge CB3 0HE, United Kingdom
and Dipartimento di Fisica Teorica, Università di Torino, and I.N.F.N., Sezione di Torino, Via Pietro Giuria 1, 10125 Torino, Italy

Kosuke Odagiri

Cavendish Laboratory, University of Cambridge, Madingley Road, Cambridge CB3 0HE, United Kingdom
(Received 25 November 1996)

We study integrated and differential rates for the production of charged Higgs bosons $H^{\pm}$ of the minimal supersymmetric standard model via b-quark-initiated subprocesses in pp collisions at the CERN Large Hadron Collider. In detail, we compute cross sections and distributions of the reactions $bU \rightarrow bDH^{+} \rightarrow bD\tau^{+}\nu_{\tau}$ $\oplus$c.c. and $bU \rightarrow bDH^{+} \rightarrow bDt\bar{b} \rightarrow bDb\bar{b}jj\oplus$c.c., for a $H^{\pm}$ scalar in the intermediate (i.e., $M^{\pm} < m_t + m_b$) and heavy (i.e., $M^{\pm} > m_t + m_b$) mass range, respectively (U and D represent generic u- and d-type light quarks). In the former case, charged Higgs boson masses up to about 145 GeV can be covered for both large and small $\tan\beta$'s. In the latter case, charged scalars can be detected for values of $M_{H^{\pm}}$ up to about 500 GeV, especially if $\tan\beta$ is large, and provided that either excellent b-tagging performances can be achieved or the high luminosity option becomes available. [S0556-2821(97)01009-6]

PACS number(s): 13.85.$-$t, 11.30.Pb, 12.60.Fr, 14.80.Cp

I. INTRODUCTION

At the CERN Large Hadron Collider (LHC) [1,2], the charged Higgs boson $H^{\pm}$ of the minimal supersymmetric standard model (MSSM) is expected (if it exists) to be copiously produced in top quark decays, via the chain $t \rightarrow bH^{\pm} \rightarrow b(\tau\nu_{\tau})$, provided that $m_t > M_{H^{\pm}} + m_b$ and that the value of $\tan\beta$ is low or high enough.[1]

The main decay modes of the $H^{\pm}$ scalar are (for $M_{H^{\pm}} < m_t + m_b$) into cs, $\tau\nu_{\tau}$, and $W^{\pm}h$ pairs, where in the last case $h \rightarrow b\bar{b}$ (h being the lightest neutral Higgs boson of the MSSM) [3]. The first decay is never dominant, whereas the second is overcome by the third in a narrow mass window right before the opening of the tb Higgs boson decay threshold, but only at very small values of $\tan\beta$. Otherwise, the branching ratio $B(H^{\pm} \rightarrow \tau\nu_{\tau})$ is the largest (around 98% for $\tan\beta > 2$), and it depends only slightly on the β angle. When $M_{H^{\pm}} > m_t + m_b$, the $H^{\pm} \rightarrow tb$ decay mode is in practice the only relevant one[2] (with a branching ratio of practically 100%).

Extensive studies and simulations for $H^{\pm}$ production at the LHC have been carried out [1,2]. Top quarks are produced in $t\bar{t}$ pairs, via $q\bar{q}$ and gg fusion, with a large cross section (around 500 pb at $\sqrt{s_{pp}} = 14$ TeV and for $m_t = 175$ GeV). The signal that has been considered in the ATLAS and CMS Technical Proposals is the one involving one top quark decaying to a charged Higgs boson, and the other decaying inclusively (i.e., either via a $H^{\pm}$ or, mostly, via a

$W^{\pm}$) into electrons and muons (and corresponding neutrinos). The charged Higgs boson is searched for by means of the leptonic signature $H^{\pm} \rightarrow \tau\nu_{\tau}$.

Since neutrinos in the final state prevent one from reconstructing the Higgs boson mass from the momenta of its decay products, the existence of $H^{\pm}$ signals in the data can be inferred only from an excess of τ production with respect to what is predicted for the standard model (SM) backgrounds (*lepton universality breaking* signal). Among the latter, one must number the irreducible ones (nonresonant τ production and $t\bar{t}$ production followed by $t \rightarrow W^{\pm}b$ and $W^{\pm} \rightarrow \tau\nu_{\tau}$) as well as the reducible ones (mainly $t\bar{t}$ where either a jet from a $W^{\pm}$ fakes a τ or a b jet decays leptonically into or fakes a τ, but also $b\bar{b}$ production followed by $b\bar{b} \rightarrow \tau$ + jets and $W^{\pm}$ + jets, with one of the jets faking a τ) [1,2]. By selecting an isolated high p_T lepton and by requiring one jet to have a high transverse energy together with one b tagging should allow one to explore a large portion of the (M_A, $\tan\beta$) plane, with a significance up to 5σ (assuming a 10 fb^{-1} integrated luminosity of the collider) [1].

It is the purpose of this paper to study other production mechanisms of charged Higgs bosons of the MSSM at the LHC, via subprocesses with b quarks in the initial state. In particular, we calculate (for a $H^{\pm}$ scalar whose mass is below the tb threshold) the signal reaction (including charge conjugation)

$$bU \rightarrow bDH^{+} \rightarrow bD\tau^{+}\nu_{\tau} \oplus \text{c.c.}, \qquad (1)$$

and the background processes

$$bU \rightarrow bD\tau^{+}\nu_{\tau} \oplus \text{c.c.} \quad \text{via intermediate } W^{\pm}, \gamma, Z, H, h, A, \qquad (2)$$

$$bU \rightarrow bD\tau^{+}\nu_{\tau} \oplus \text{c.c.} \quad \text{via intermediate } W^{\pm}, g, \qquad (3)$$

---

[1]The minimum of the $t \rightarrow bH^{\pm}$ decay rate is at about $\tan\beta = 6$.

[2]In the above discussion and throughout this paper we have assumed that the mass scale of the supersymmetric particles is above the $H^{\pm}$ mass, such that only decays into ordinary matter are here considered.

$$U\bar{D} \rightarrow b\bar{b}\tau^+\nu_\tau \oplus \text{c.c.} \quad \text{via intermediate } W^\pm, g, \quad (4)$$

where $U(D)$ represents a generic u- (d-)type light quark (i.e., u, d, s, and c) found inside the proton and H,h,A are the three neutral Higgs bosons of the MSSM. For a heavy $H^\pm$, we consider the production and decay chain (again including charge conjugation)

$$bU \rightarrow bDH^+ \rightarrow bD\bar{b}t \rightarrow bD\bar{b}b\text{jj} \oplus \text{c.c.}, \quad (5)$$

assuming that, because of the spectacular signature that is produced in the final state, background processes can easily be kept under control. In reactions (1)–(3) and (5) we treat the initial b quark as a constituent of the proton with the appropriate momentum fraction distribution $f_{b/p}(x,Q^2)$, as given by our default set of partonic structure functions.

The relevance of these reactions can be understood if one considers that at the typical (partonic) energies of the LHC the content of b quarks inside the colliding protons is very much enhanced, compared to lower energy hadronic scatterings (such as, e.g., at the Fermilab Tevatron), the presence of b quark in initial, virtual, and final states means that many of the MSSM Yukawa couplings of the Higgs bosons of the theory are increased for large values of $\tan\beta$, and the vertex-tagging performances of the LHC detectors are expected to become almost ''ideal'' by the time the machine starts operations, thus allowing one to greatly reduce the QCD background of light quark and gluon jets.

Finally, we also stress that b-quark initiated processes at LHC energies have already been demonstrated to be important in the case of neutral MSSM Higgs boson production, especially at large $\tan\beta$'s and for intermediate masses of the scalars [4], as well as in the case of charged Higgs boson production, via the reaction $g\bar{b} \rightarrow H^+\bar{t} \oplus \text{c.c.}$ [5].

The plan of this paper is as follows. In the next section we give some details of the calculation and list the values adopted for the various parameters. Section III is devoted to a discussion of the results. Conclusions are in Sec. IV. In the Appendix we write down the amplitudes squared of the signal processes.

II. CALCULATION

To calculate processes (1)–(5) we have used the spinor techniques described in Refs. [6–8]. The FORTRAN codes we have produced have been counterchecked against the outputs of MADGRAPH [9], which incorporates the HELAS subroutines [10]. We have always found perfect agreement between the two kind of programs. The codes written using the helicity formalism of Refs. [6–8] have also been tested for gauge invariance. Furthermore, in order to speed up the numerical evaluations in Monte Carlo simulations, the matrix elements for the signal processes (1) and (5) have been computed using the textbook method of taking the trace of the γ matrices, with the help of FORM [11]. The analytical expressions obtained in this way are very simple, so that we do reproduce them here (see the Appendix). They have been eventually implemented and their numerical results agree with those of the other codes. The integrations over the phase space have been performed using VEGAS [12].

The tree-level Feynman diagrams that one needs for com-

puting processes (1)–(5) are given in Figs. 1(a)–1(d).[3] Note that the virtual particle content of the diagrams is explicitly indicated in Fig. 1 for all reactions.

Concerning the values of the various parameters entering in the computation of processes (1)–(5), we have proceeded as follows. First, we have set up the mass scale of the super-symmetric partners of ordinary matter well above the energy reach of the LHC, such that we can neglect their contribution in our calculations. To further simplify the discussion, we have assumed a universal soft supersymmetry-breaking mass [13,14]

$$m_{\tilde{u}}^2 = m_{\tilde{d}}^2 = m_{\tilde{q}}^2, \quad (6)$$

and negligible mixing in the top-squark and bottom squark mass matrices:

$$A_t = A_b = \mu = 0. \quad (7)$$

One-loop corrections to the masses of the MSSM neutral CP-even Higgs bosons and to the mixing angle α are introduced via the parameter ε of Ref. [15], given by (neglecting the b mass)

$$\varepsilon = \frac{3e^2}{8\pi^2 M_{W^\pm}^2 \sin^2\theta_W} m_t^4 \ln\left(1 + \frac{m_{\tilde{q}}^2}{m_t^2}\right), \quad (8)$$

where $e^2 = 4\pi\alpha_{\text{em}}$. One then gets [13]

$$M_{h,H}^2 = \frac{1}{2}[M_A^2 + M_Z^2 + \varepsilon/\sin^2\beta]$$
$$\pm\{[(M_A^2 - M_Z^2)\cos2\beta + \varepsilon/\sin^2\beta]^2$$
$$+ (M_A^2 + M_Z^2)^2\sin^2 2\beta\}^{1/2}, \quad (9)$$

and

$$\tan2\alpha = \frac{(M_A^2 + M_Z^2)\sin2\beta}{(M_A^2 - M_Z^2)\cos2\beta + \varepsilon/\sin^2\beta}. \quad (10)$$

For the MSSM charged Higgs boson masses we have maintained the tree-level relations

$$M_{H^\pm}^2 = M_A^2 + M_{W^\pm}^2, \quad (11)$$

since one-loop corrections are small compared to those for the neutral Higgs boson [14].

In the numerical calculations presented in the next section we have adopted the following values for the electromagnetic coupling constant and the weak mixing angle: $\alpha_{\text{em}} = 1/128$ and $\sin^2\theta_W = 0.2320$. The strong coupling constant α_s, which appears at next-to-leading order in the com-

---

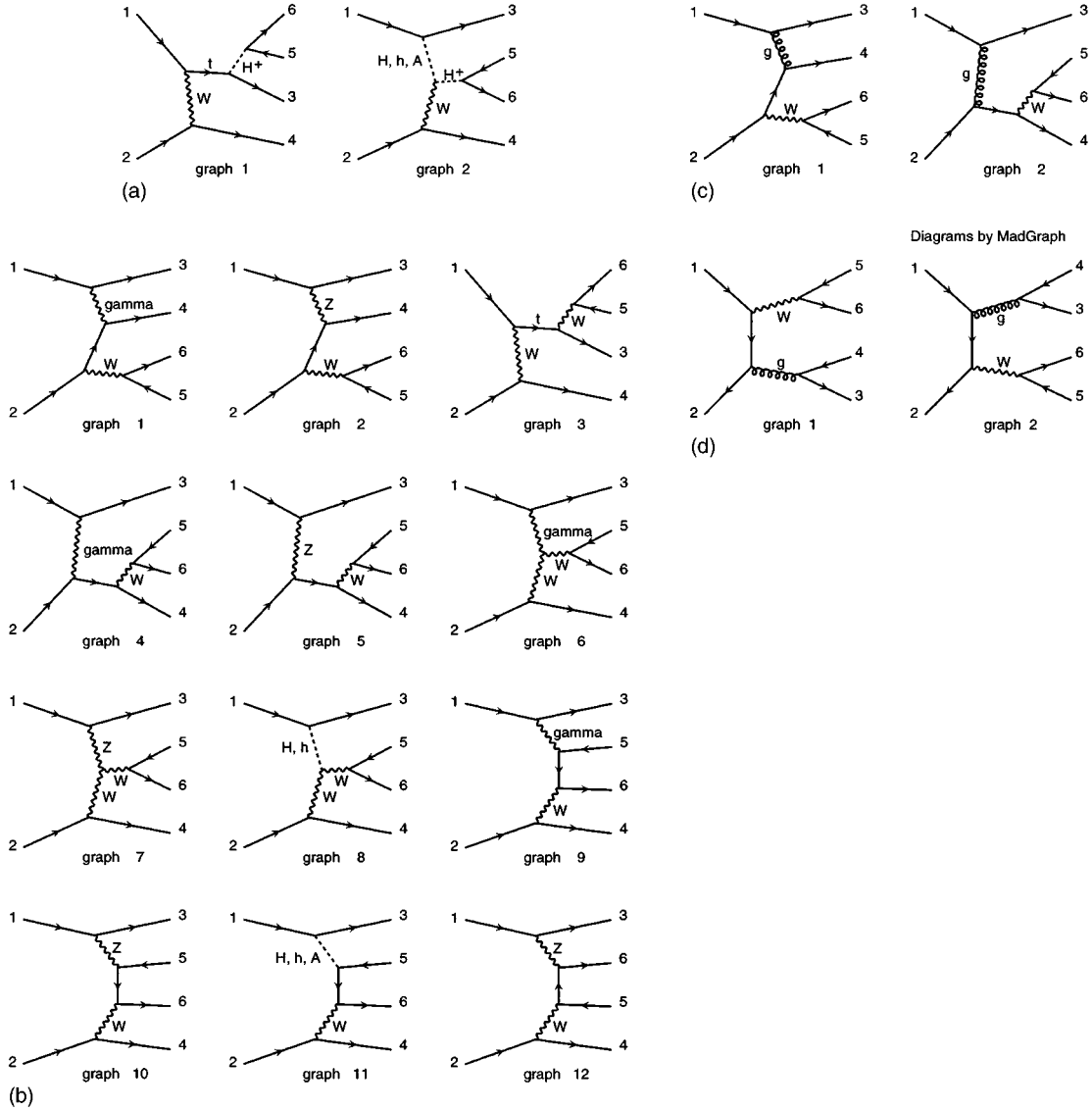[3]The c.c. diagrams can be obtained by simple crossing and time inversion of fermion lines.

FIG. 1. Feynman diagrams contributing at lowest order to the subprocess $bU \rightarrow bD\tau^+\nu_\tau \oplus$c.c.: (a) via $H^\pm$ resonant graphs; (b) via $W^\pm$ resonant graphs and through EW only; (c) via $W^\pm$ resonant graphs and through QCD interactions; and to the subprocess $U\bar{D} \rightarrow b\bar{b}\tau^+\nu_\tau \oplus$c.c.: (d) via $W^\pm$ resonant graphs and through QCD interactions. Here, U and D represent any of the light quarks u, d, s, and c. The labeling of the particles in the initial state corresponds to their ordering in the left-hand side of Eqs. (1)–(5), whereas for the final state it refers to the right-hand side of Eqs. (1)–(4) and to the stage of on-shell top quark production in Eq. (5). The PostScript version of the Feynman graphs has been produced using MADGRAPH [9].

putation of the charged Higgs boson decay width (see Ref. [3]) and enters in some of the production mechanisms, has been evaluated at two loops, with $\Lambda_{\overline{\mathrm{MS}}}^{(4)} = 230$ MeV, and with the number of active flavors N_f (and the corresponding $\Lambda_{\overline{\mathrm{MS}}}^{(N_f)}$) calculated according to the prescription of Ref. [16] at the scale $Q^2 = s$.

For the gauge boson masses and widths we have taken $M_Z = 91.1888$ GeV, $\Gamma_Z = 2.5$ GeV, $M_{W^\pm} = 80.23$ GeV, and $\Gamma_{W^\pm} = 2.08$ GeV, while for the fermion masses we have used $m_e = m_{\nu_e} = m_{\nu_\mu} = m_{\nu_\tau} = 0$, $m_\mu = 0.105$ GeV, $m_\tau = 1.78$ GeV, $m_u = m_d = m_s = m_c = 0$, $m_b = 4.25$ GeV, and $m_t = 175$ GeV, with all widths equal to zero except for Γ_t. We have calculated this at the tree level within the MSSM, using the expressions given in Refs. [17,18]. The universal supersymmetry-breaking squark mass is in the numerical

analysis $m_{\tilde{q}} = 1$ TeV and the LHC center-of-mass (c.m.) energy is $\sqrt{s}_{pp} = 14$ TeV. Finally, throughout the paper we have always used Martin-Roberts-Stirling set A (MRSA) [20][4] as

_____

[4]Actually, we have done so only in the production processes [those represented by the graphs in Figs. 1(a)–1(d)]. In fact, for process (5), to describe the decay chain $t \rightarrow bW^\pm \rightarrow b$jj, we have used a narrow width approximation (NWA) for the top quark, by implementing the decay formulas as given in Ref. [19]. This has been done in order to avoid a large consumption of CPU time in computing exactly a 2→6 partonic process convoluted with initial structure functions and in presence of multiple resonant peaks in different regions of the phase space. We are confident that such an approximation does not spoil the validity of our conclusions.
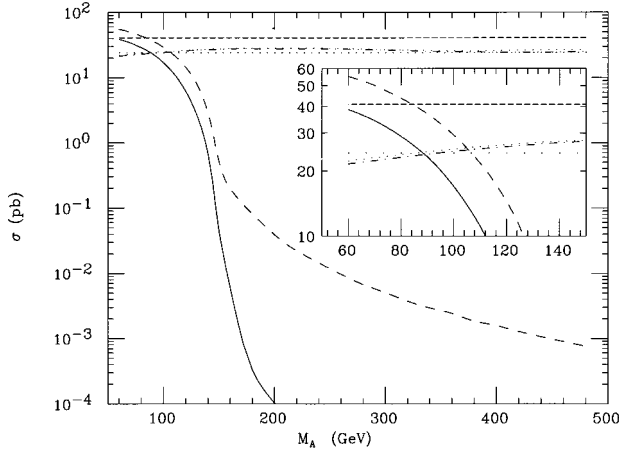
FIG. 2. Cross section of the four processes (1)–(4), at the LHC for $\sqrt{s}_{pp} = 14$ TeV, in the region 60 GeV$\lesssim M_A \lesssim$480 GeV and for two different values of tanβ [in the case of processes (1) and (2)]. In the top right hand plot we enlarge the region 60 GeV $\lesssim M_A \lesssim$150 GeV. Solid line: process (1) with tanβ=1.5. Dashed line (large spacing): process (1) with tanβ=30. Dotted line (large spacing): process (2) with tanβ=1.5. Dot-dashed line: process (2) with tanβ=30. Dashed line (small spacing): process (3). Dotted line (small spacing): process (4). The cut $p_T^{\text{final}} > 10$ GeV has been applied to all particles in the final states, except for neutrinos. The structure function set MRSA has been used.

the default set of partonic distributions, with the same α_s and $\Lambda_{\overline{\text{MS}}}^{(4)}$ as above, where $\overline{\text{MS}}$ denotes the modified minimal subtraction scheme.

III. RESULTS

As it is impractical to cover all possible regions of the MSSM parameter space (M_A,tanβ), we have decided to concentrate here on the two representative (and extreme) values tanβ=1.5 and 30, and on masses of the pseudoscalar Higgs boson A in the range 60 GeV $\lesssim M_A \lesssim$500 GeV. The large bibliography existing on the MSSM Higgs boson decay phenomenology allows one to easily extrapolate our results to other values of tanβ [21].

In Fig. 2 we display the total cross sections at the LHC for processes (1)–(4), for values of M_A up to 480 GeV and for the two above-mentioned tanβ's (note that a minimum transverse momentum of 10 GeV is required for all detectable particles in the final states of all processes). The relevant feature of Fig. 2 is that process (1) has rather large rates, of the same order as the backgrounds (2)–(4). This is particularly true below $M_A \approx 120$ GeV (which corresponds to $M_{H^\pm} \approx 145$ GeV, small window in the upper right corner of Fig. 2), and more for large than for small values of tanβ. The latter aspect is a consequence of the fact that the branching ratio (BR) of the charged Higgs boson into $\tau\nu_\tau$ pairs is enhanced at tanβ=30, a value for which the cs channel is negligible (see Ref. [3]). An additional contribution comes from graph 2 in Fig. 1(a), which involves Yukawa vertex contributions proportional to tanβ. However, the largest part of the signal cross section is due to graph 1 in Fig. 1(a), because of a resonant top quark decay. The steep decrease of the signal rates around $M_A \approx 150$ GeV is due to the opening

of the $H^\pm \to tb$ off-shell decay channel (see Refs. [3,22]).

Concerning the background processes (2)–(4), one notices that they are "roughly" independent of M_A and tanβ. This is obvious for processes (3) and (4), as they proceed through SM graphs [Figs. 1(c) and 1(d)], whereas for process (2) this indicates that the contributions to the total cross section due to interactions involving MSSM vertices [that is, graphs 8 and 11 in Fig. 1(b)] are irrelevant (even at tanβ =30). We also notice that, unlike processes (2) and (3), reaction (4) is not an irreducible background, as its final state is different from that of the signal. Nevertheless, as it includes two bottom quarks among the produced particles, the probability that its final signature be the same as the signal is (neglecting the misidentification of light flavor quarks as b's as well as correlations between the two possible tags) $P = 1 - B$, where $B = 2\varepsilon_b - \varepsilon_b^2$, ε_b being the efficiency of tagging one b jet. Hence, better b tagging leads to lower detection rates of the background process (4).

Therefore, from the figure it is clear that, in principle, a large excess of τ events could be produced in the scattering process, provided that $M_A \lesssim 120$–130 GeV (at large tanβ's such an interval can be possibly extended up to 130–140 GeV). The possibilities of actually disentangling the signal depend strongly on the detector performances of the LHC, in particular in recognizing the displaced vertex in jets which originate from b quarks.[5] In fact, the signature that one would look for is $bj\tau\not{E}_T X$, where $\not{E}_T$ represents the missing (transverse) energy due to the neutrino escaping the detectors and j is the jet arising from the light parton scattered in the proton. In order to quantify the significance of the signals we list in Table I the total cross sections of processes (1)–(4) (as read from Fig. 2) for $M_A = 60(80)[100]\{120\}$ GeV (corresponding to $M_{H^\pm} = 100(113)[128]\{144\}$ GeV), for both values of tanβ=1.5 and 30, multiplied by the b-tagging efficiencies and by the yearly luminosity, $\int \mathcal{L}dt = 10$ fb^{-1} (the minimum considered for the final collider design). Furthermore, we also compute the relative excess of signal events S with respect to the total background B, as $\Delta = S/B \times 100$. For the microvertex performances, we have adopted the following three reference values: $\varepsilon_b = 1.0$, 0.75, and 0.5.[6] From the numbers given there one deduces that the relative excess of $H^\pm$ events is always quite large, especially at tanβ=30, and that the absolute statistics is huge, between $\sim 10^4$ and 10^5 signal events per year. In our opinion then, given the expected performances of the LHC detectors [1,2], such signals could well be detectable soon after turning on the machine. Moreover, we stress that, as the total luminosity gets larger, the significance of the signal with respect to the total background will increase further.

However, before drawing optimistic conclusions, one has to carefully consider first the kinematic properties of processes (1)–(4), as the LHC detectors will have a finite coverage (for example, in pseudorapidity η and transverse momentum p_T of the visible particles). Hence, we have plotted

---

[5]We believe that hadronic τ decays can be easily distinguished from quark and gluon jets.

[6]In first approximation, we assume that the rejection factor for misidentification of light quarks and gluons as b jets is large enough, that we can neglect the reducible QCD background here.

TABLE I. Number of events for signal (1) and total background (2)–(4), at the LHC with c.m. energy $\sqrt{s_{pp}} = 14$ TeV, for $M_A = 60(80)[100]\{120\}$ GeV, and $\tan\beta = 1.5$ and 30, assuming the yearly luminosity $\int \mathcal{L} dt = 10$ fb^{-1} and the b-tagging efficiencies $\varepsilon_b = 1.0$, 0.75, and 0.5 (first, second, and third row, respectively), together with the relative excess of signal events with respect to the total background.

	$N_{ev}(bj\tau \not{E}_T X)$	
S	B	Δ
$386(289)[170]\{62\} \times 10^3$	$630(645)[654]\{671\} \times 10^3$	$61(45)[26]\{9\}\%$
$289(217)[127]\{47\} \times 10^3$	$488(498)[506]\{518\} \times 10^3$	$59(44)[25]\{9\}\%$
$193(145)[85]\{31\} \times 10^3$	$375(383)[387]\{396\} \times 10^3$	$51(38)[22]\{8\}\%$
	$\tan\beta = 1.5$	
$551(436)[294]\{145\} \times 10^3$	$623(639)[651]\{672\} \times 10^3$	$88(68)[45]\{22\}\%$
$413(327)[220]\{109\} \times 10^3$	$483(494)[504]\{519\} \times 10^3$	$86(66)[44]\{21\}\%$
$275(218)[147]\{73\} \times 10^3$	$372(380)[386]\{396\} \times 10^3$	$74(57)[38]\{18\}\%$
	$\tan\beta = 30$	
	$M_A = 60(80)[100]\{120\}$ GeV	
$p_T^{final} > 10$ GeV		MRSA
$\sqrt{s_{pp}} = 14$ TeV		$\int \mathcal{L} dt = 10$ fb^{-1}

in Figs. 3 and 4, the differential spectra in the above variables for both signal and background processes. If one assumes that the phase-space region that can be covered experimentally is approximately the one delimited by the requirements $|\eta(b,\tau,j)| < 3$ and $p_T(b,\tau,j) > 20$ GeV [1,2], then one can easily verify that most signal events are contained in the detectable region (we have checked that also in the case $M_A = 60$ GeV one gets distributions similar to those of Figs. 3 and 4). This is true for background events as well, process (4) being possibly the only exception [in the pseudorapidity spectra, upper left corner in Figs. 4(a) and 4(b)]. In the end then, one should expect that usual selection criteria will not alter the conclusions that were previously extracted from the total rates of Table I.

If the charged Higgs boson mass is above the tb threshold, $H^\pm$ scalars could reveal themselves via the production and decay mechanism (5). For a heavy $H^\pm$ boson, we consider then the signature $bbbjjjX$, where b represents either a quark or the corresponding antiquark, and j a jet that does not show a displaced vertex. In this case, the final state that should be detected is much more complicated than that of an intermediate mass $H^\pm$ boson, as it is made up of six jets. Nevertheless, the complex resonant structure of process (5) brings some advantages to the tagging procedure. In fact, on the one hand, three vertex tags are now required (which introduce the suppression factor ε_b^3), and in a high hadronic multiplicity environment, in addition, complications arise from the combinatorics of the jets. On the other hand, the kinematics of the jets in the final state is highly constrained, since (i) one of three possible jj combinations must reproduce the $W^\pm$ mass (i.e., $M_{jj} \approx M_{W^\pm}$); (ii) one of the nine possible $b$jj combinations must reproduce at the same time the t and $W^\pm$ masses (i.e., $M_{bjj} \approx m_t$, with $M_{jj} \approx M_{W^\pm}$). In this respect, note that in the decay chain $t \rightarrow bW^\pm \rightarrow bjj$ we do not need to consider intermediate $H^\pm$ contributions, as in the heavy $M_{H^\pm}$ range the $t \rightarrow bH^\pm$ is forbidden.

The total cross section for process (5) is displayed in Fig. 5, as a function of the A mass in the range 140 GeV $\lesssim M_A \lesssim 480$ GeV (for both $\tan\beta = 1.5$ and 30). Both the $t \rightarrow bW^\pm$ and $W^\pm \rightarrow jj$ branching ratios are included. For comparison, we also reproduce from Fig. 1 the rates for process (1). A first feature that is worth noticing in Fig. 5 is that again the rates of process (5) for $\tan\beta = 30$ are larger than those for $\tan\beta = 1.5$. In practice, there are two opposite effects which take place: on the one hand, at small $\tan\beta$, the $B(H^\pm \rightarrow tb)$ is larger whereas, on the other hand, at large $\tan\beta$, the contribution from graph 2 in Fig. 1(a) is enhanced by couplings proportional to $\tan\beta$ itself.[7] Of the two, it is the second that dominates over most of the $M_{H^\pm}$ range. Furthermore, at large $\tan\beta$'s, processes (1) and (5) yield rates of the same order for $M_A \gtrsim 200$ GeV, such that in this case they can be contemporaneously exploited in searching for $H^\pm$ signals. This is not true at small $\tan\beta$. In general, it should be noted that in Fig. 5 one is dealing with total rates that are more than two orders of magnitude smaller that for the case of an intermediate mass $H^\pm$ boson in the $\tau\nu_\tau$ channel. Nevertheless, as a starting point one can rely on ~ 10–100 signal events produced via $H^\pm \rightarrow tb$ per year (for the same luminosity as above). Clearly, in this case the need for a high value of ε_b is crucial. For example, a vertex-tagging efficiency of 50% reduces the production rates by a factor of 8.

In Fig. 6 we plot the spectrum in the sum of the invariant mass of all possible $bbjj$ combinations entering in process (5).[8] The values of M_A considered here as a reference are 200, 300, 400, and 500 GeV. Since at least one of the $bbjj$ systems is made up by the decay products of the charged Higgs boson, a peak should possibly appear in the distributions (at $M_{H^\pm} = 215$, 311, 408, and 506 GeV, respectively), on top of the combinatorial background. Indeed, the resonant

---

[7]Also note that at the same time, since $M_{H^\pm} > m_t + m_b$, the first graph in Fig. 1(a) is no longer resonant.

[8]Note that in our NWA approach we automatically obtain $M_{bjj} \equiv m_t$ for the right three jet combination. In the case of the $W^\pm$ decay we have adopted the "conservative" requirement $|M_{jj} - M_{W^\pm}| < 15$ GeV.
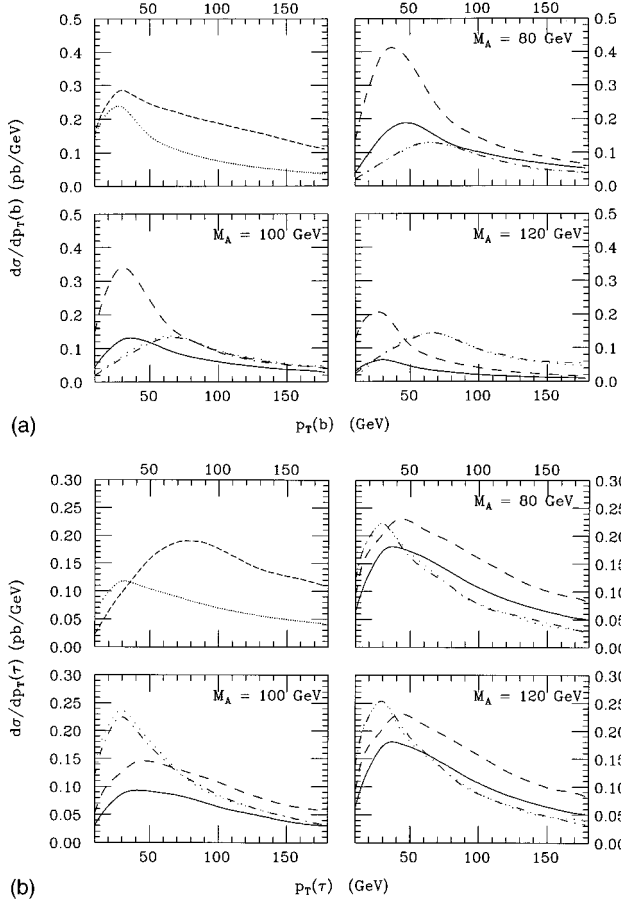
FIG. 3. Differential distribution in transverse momentum of the b quark (a) and of the τ lepton (b) for the four processes (1)–(4), at the LHC for $\sqrt{s}_{pp} = 14$ TeV, for the following selection of masses $M_A = 80, 100, 120$ GeV and for two different values of $\tan\beta$ [in the case of processes (1) and (2)]. Solid line: process (1) with $\tan\beta = 1.5$. Dashed line (large spacing): process (1) with $\tan\beta = 30$. Dotted line (large spacing): process (2) with $\tan\beta = 1.5$. Dot-dashed line: process (2) with $\tan\beta = 30$. Dashed line (small spacing): process (3). Dotted line (small spacing): process (4). Please note that the two curves corresponding to process (2) are practically indistinguishable. The cut $p_T^{\text{final}} > 10$ GeV has been applied to all particles in the final states, except for neutrinos. The structure function set MRSA has been used.
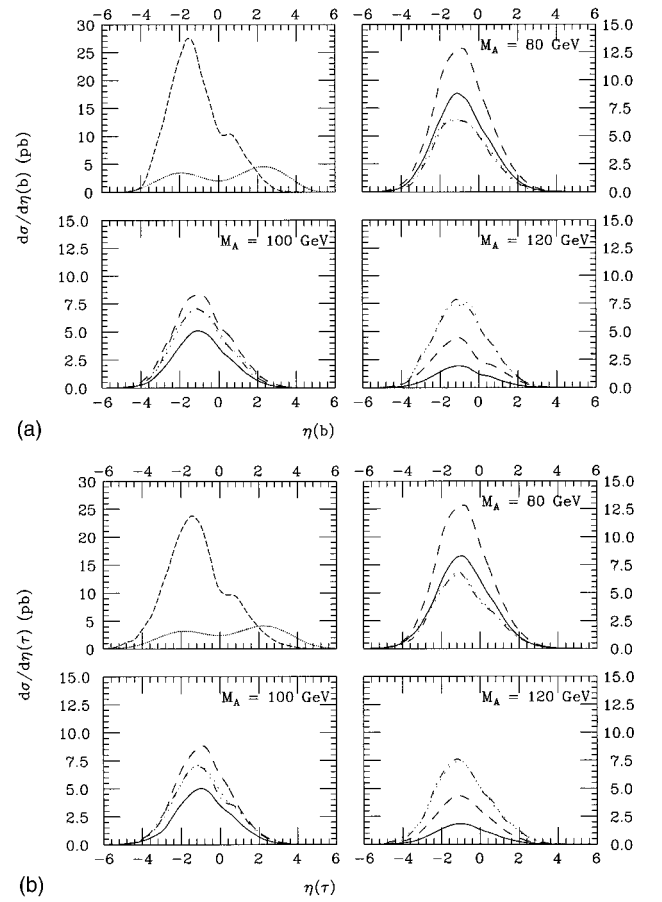
FIG. 4. Differential distribution in pseudorapidity of the b quark (a) and of the τ lepton (b) for the four processes (1)–(4), at the LHC for $\sqrt{s}_{pp} = 14$ TeV, for the following selection of masses $M_A = 80, 100, 120$ GeV and for two different values of $\tan\beta$ [in the case of processes (1) and (2)]. Solid line: process (1) with $\tan\beta = 1.5$. Dashed line (large spacing): process (1) with $\tan\beta = 30$. Dotted line (large spacing): process (2) with $\tan\beta = 1.5$. Dot-dashed line: process (2) with $\tan\beta = 30$. Dashed line (small spacing): process (3). Dotted line (small spacing): process (4). Please note that the two curves corresponding to process (2) are practically indistinguishable. The cut $p_T^{\text{final}} > 10$ GeV has been applied to all particles in the final states, except for neutrinos. The structure function set MRSA has been used.

peaks are quite sharp (the $H^\pm$ widths are approximately, for the above values of mass: 0.84, 3.03, 5.20, and 7.20 GeV at both $\tan\beta$ values), and clearly visible. However, the total number of events in the region, say, $|M_{bbjj} - M_{H^\pm}| < 25$ GeV is, for $\tan\beta = 30$: 25(10)[3], 9(4)[1], 4(2)[0.4], and 2(1) [0.2] (for the four masses above), for 10 fb^{-1} per year of luminosity, assuming $\varepsilon_b = 1(0.75)[0.5]$. Therefore, at least for not too heavy $H^\pm$'s and high b-tagging performances, one could possibly look for $H^\pm$ signals in the tb channel at large $\tan\beta$'s. Certainly, if the high luminosity option $\int \mathcal{L} dt = 100$ fb^{-1} can be achieved at the LHC, things would be very optimistic, as in a few years of running, even the very heavy mass region could be scanned. At small values of $\tan\beta$ one has to consider rates that are typically smaller by one order of magnitude, rendering Higgs boson detection much more difficult.

Finally, in Fig. 7, we show the differential spectrum in transverse momentum of the various bbjj combinations that can be reconstructed from process (5), for the same values of M_A as above. We notice that from the figure it is clear that the p_T spectrum of the Higgs boson decay products is significantly hard (because of the large mass of the scalar), a feature that could well help in disentangling heavy $H^\pm$ boson signals, especially considering that the ordinary QCD background in six-jet events has quite a soft transverse momentum distribution.

IV. CONCLUSIONS

In this paper we have studied, within the MSSM, a new production mechanism of charged Higgs bosons $H^\pm$ at LHC energies, via b-quark-initiated interactions. Two possible Higgs signatures have been considered, depending on
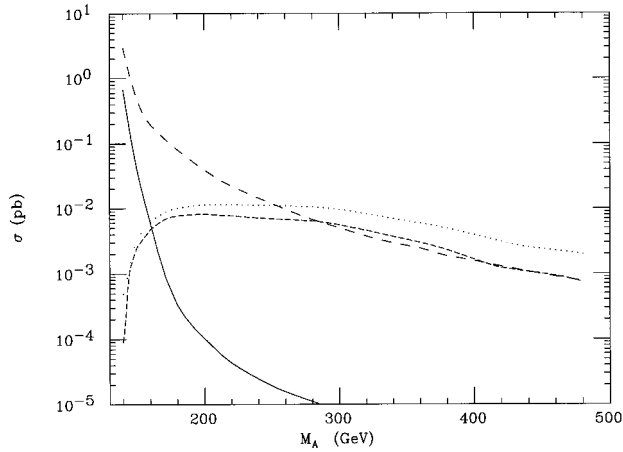
FIG. 5. Cross section of processes (1) and (5), at the LHC for $\sqrt{s_{pp}}=14$ TeV, in the region 140 GeV$\lesssim M_A \lesssim$480 GeV and for two different values of $\tan\beta$. Solid line: process (1) with $\tan\beta=1.5$. Dashed line (large spacing): process (1) with $\tan\beta=30$. Dashed line (small spacing): process (5) with $\tan\beta=1.5$. Dotted line: process (5) with $\tan\beta=30$. The cut $p_T^{\text{final}}>10$ GeV has been applied to all particles in the final states, including the top quark decay products. The structure function set MRSA has been used.

whether the mass $M_{H^\pm}$ is below or above $m_t+m_b\approx180$ GeV.

In the first case, by exploiting one vertex tag on one b jet in the final state, the Higgs boson decay channel $H^\pm\to\tau\nu_\tau$ should be identifiable as a clear excess in the number of τ events with respect to the rates predicted by the non-SUSY backgrounds, provided that $M_A\lesssim130$ GeV (i.e., $M_{H^\pm}\lesssim144$ GeV), both at large and small values of $\tan\beta$. Also, the absolute number of signal events is statistically very large. In this mass range, a careful treatment of various background sources has been performed.

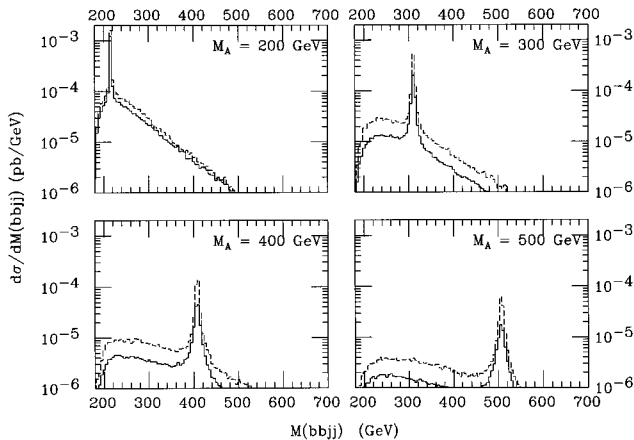In the second case, the channel $H^\pm\to tb\to bb$jj (via had-

FIG. 6. Differential distribution in invariant mass of the bbjj systems for process (5), at the LHC for $\sqrt{s_{pp}}=14$ TeV, for the following selection of masses $M_A=200,300,400,500$ GeV, for $\tan\beta=1.5$ (solid line) and 30 (dashed line). The cut $p_T^{\text{final}}>10$ GeV has been applied to all particles in the final states, including the top boson decay products. Bins are 5 GeV wide. The structure function set MRSA has been used.
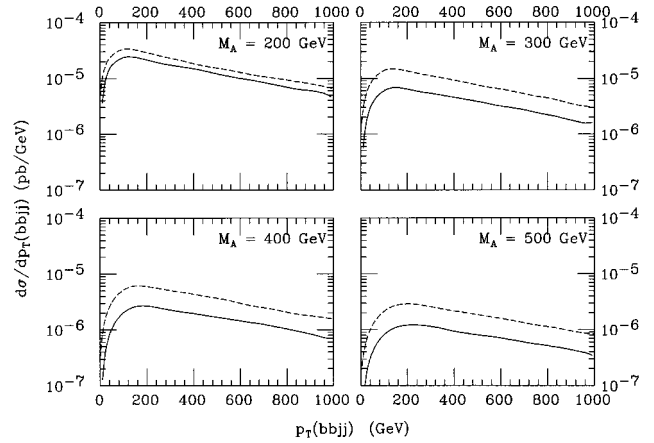

FIG. 7. Differential distribution in transverse momentum of the $bbjj$ systems for process (5), at the LHC for $\sqrt{s_{pp}}=14$ TeV, for the following selection of masses $M_A=200,300,400,500$ GeV, for $\tan\beta=1.5$ (solid line) and 30 (dashed line). The cut $p_T^{\text{final}}>10$ GeV has been applied to all particles in the final states, including the top quark decay products. The structure function set MRSA has been used.

ronic $W^\pm$ decays of the top quark) has been considered. The signature arising from heavy $H^\pm$ decays is complicated (a six-jet final state involving three b jets) and only a small number of events is expected. Nonetheless, the resonant behavior of the t, $H^\pm$, and $W^\pm$ decay products should allow one to eliminate the ordinary QCD background in light quark and gluon jets, although (in the heavy mass range) a signal-to-background analysis has not been performed. In general, if high b-tagging performances can be achieved and/or the high luminosity option becomes available at the LHC, $H^\pm$ scalars with masses up to 500 GeV could well be searched for, as the combinatorial background does not spoil the form of the Higgs boson peaks. This is, however, true only for large values of $\tan\beta$, since for low $\tan\beta$'s the event rates are smaller by one order of magnitude.

The range between $M_A\approx130$–140 GeV and up to the opening of the tb decay threshold is extremely difficult to cover, as rates in the $\tau\nu_\tau$ channel drastically decrease well below the background rates and at the same time the off-shell tb channel has a very small statistics.

Finally, we stress that, before drawing any firm conclusion from our results, one should include a realistic simulation of the expected performances of the LHC detectors and that, in the heavy mass range $M_{H^\pm}>m_t+m_b$, a detailed background study (including all the hadronization effects in a six-jet final state, an analysis which was beyond our capabilities) should be performed. Nevertheless, we believe that the matter presented here would deserve experimental attention when proceeding to the various simulations of the MSSM Higgs phenomenology at the CERN hadron collider.

ACKNOWLEDGMENTS

APPENDIX

In this additional section we write down in analytic form the matrix element for the signal processes. As an example, we reproduce that of the reaction $bU \rightarrow bDH^+ \rightarrow bD\tau^+\nu_\tau$

$\oplus$c.c.. However, by replacing $\tau \rightarrow t$ and $\nu_\tau \rightarrow b$, one can easily obtain that for top-bottom (on-shell) production. In fact, we have used a narrow width approximation for the top quark when this is produced from the $H^\pm$ splitting, by computing the exact amplitude squared for $bU \rightarrow bDH^+ \rightarrow bDt\bar{b} \oplus$c.c. and by interfacing this with a SUBROUTINE implementing the top quark decay formulas into $bW^\pm$ pairs as given in Ref. [19].

The matrix element squared (summed or averaged over the final or initial spins and colors) for the process $bU \rightarrow bDH^+ \rightarrow bD\tau^+\nu_\tau$ reads as

$$|\mathcal{M}|^2 = |\mathcal{M}_0|^2 |P_H|^2 |P_W|^2 (|\mathcal{M}_t|^2 + |\mathcal{M}_\phi|^2 + 2|\mathcal{M}_t^* \mathcal{M}_\phi|),$$

with

$$|\mathcal{M}_0|^2 = (g^4/2M_W^2)^2 [p_\tau \cdot p_{\nu_\tau}(m_\tau^2 \tan^2\beta + m_{\nu_\tau}^2 \cot^2\beta) - 2m_\tau^2 m_{\nu_\tau}^2],$$

$$P_H = (p_H^2 - M_H^2 + iM_H\Gamma_H)^{-1}, \quad P_W = (p_W^2 - M_W^2 + iM_W\Gamma_W)^{-1},$$

$$|\mathcal{M}_t|^2 = 2|P_t|^2 p_{b,\text{in}} \cdot p_U [2m_b^2(m_t^2 + p_{b,\text{out}} \cdot p_t \tan^2\beta)p_t \cdot p_D + (m_t^4 \cot^2\beta - m_b^2 p_t^2 \tan^2\beta)p_{b,\text{out}} \cdot p_D],$$

$$|\mathcal{M}_\phi|^2 = m_b^2 \sec^2\beta(2p_H \cdot p_D p_H \cdot p_U - p_H^2 p_U \cdot p_D)[m_b^2(|P_{H_0,h_0}|^2 - |P_{A_0}|^2) + p_{b,\text{out}} \cdot p_{b,\text{in}}(|P_{H_0,h_0}|^2 + |P_{A_0}|^2)],$$

$$2|\mathcal{M}_t^* \mathcal{M}_\phi| = m_b^2 \sec\beta(\{\text{Re}[P_t^*(P_{H_0,h_0} - P_{A_0})]m_t^2 \cot\beta - \text{Re}[P_t^*(P_{H_0,h_0} + P_{A_0})]m_b^2 \tan\beta\}(p_{b,\text{out}} \cdot p_D p_H \cdot p_U + p_{b,\text{out}} \cdot p_U p_H \cdot p_D$$

$$- p_{b,\text{out}} \cdot p_H p_U \cdot p_D) + \{\text{Re}[P_t^*(P_{H_0,h_0} - P_{A_0})]m_b^2 \tan\beta + \text{Re}[P_t^*(P_{H_0,h_0} + P_{A_0})](m_t^2 \cot\beta + 2p_{b,\text{in}} \cdot p_{b,\text{out}} \tan\beta)\}$$

$$\times (p_{b,\text{in}} \cdot p_D p_H \cdot p_U + p_{b,\text{in}} \cdot p_U p_H \cdot p_D - p_{b,\text{in}} \cdot p_H p_U \cdot p_D) + 2\text{Re}[P_t^*(P_{H_0,h_0} + P_{A_0})]\tan\beta(p_{b,\text{in}} \cdot p_U p_{b,\text{out}} \cdot p_H p_U \cdot p_D$$

$$- p_{b,\text{in}} \cdot p_U p_{b,\text{out}} \cdot p_D p_U \cdot p_H + p_{b,\text{in}} \cdot p_D p_U \cdot p_{b,\text{out}} p_U \cdot p_H - p_{b,\text{in}} \cdot p_H p_U \cdot p_{b,\text{out}} p_U \cdot p_D)$$

$$- 2\epsilon_{\mu\nu\lambda\sigma} p_{b,\text{in}}^\mu p_{b,\text{out}}^\nu p_U^\lambda p_D^\sigma \{\text{Im}(P_t^* P_{A_0})m_b^2 \tan\beta - \text{Im}(P_t^* P_{H_0,h_0})m_t^2 \cot\beta$$

$$- \text{Im}[P_t^*(P_{H_0,h_0} + P_{A_0})]\tan\beta(p_{b,\text{in}} \cdot p_{b,\text{out}} - p_{b,\text{in}} \cdot p_U + p_{b,\text{out}} \cdot p_U)\}).$$

Here, we have set $m_U = m_D = 0$, $p_t = p_{b,\text{in}} + p_W = p_{b,\text{out}} + p_H$, and

$$P_t = (p_t^2 - m_t^2 + im_t\Gamma_t)^{-1},$$

$$P_{H_0,h_0} = \cos\alpha\sin(\beta - \alpha)(p_\phi^2 - M_{H_0}^2 + iM_{H_0}\Gamma_{H_0})^{-1} + \sin\alpha\cos(\beta - \alpha)(p_\phi^2 - M_{h_0}^2 + iM_{h_0}\Gamma_{h_0})^{-1},$$

$$P_{A_0} = \sin\beta(p_\phi^2 - M_{A_0}^2 + iM_{A_0}\Gamma_{A_0})^{-1},$$

$$p_H = p_\tau + p_{\nu_\tau}, \quad p_\phi = p_{b,\text{in}} - p_{b,\text{out}}, \quad p_W = p_U - p_D,$$

where $p_{b,\text{in}}$, p_U, $p_{b,\text{out}}$, p_D, p_τ, and p_{ν_τ} are the external momenta (incoming or outgoing in the initial or final state). Note that the symbols Re and Im refer to the real and imaginary part of a complex number, respectively, and that $\epsilon_{\mu\nu\lambda\sigma}$ is the Levi-Cività tensor ($\epsilon_{0123} = 1$). Finally, by exchanging $p_{b,\text{in}} \leftrightarrow -p_{b,\text{out}}$ and $\epsilon_{\mu\nu\lambda\sigma} \leftrightarrow -\epsilon_{\mu\nu\lambda\sigma}$, one can obtain the amplitude squared for $\bar{b}U$ fusion, and by relabeling $U \leftrightarrow D$, those for the bD- and $\bar{b}D$-initiated reactions.

[1] CMS Technical Proposal, Report No. CERN/LHC/94-43 LHCC/P1, 1994 (unpublished).

[2] ATLAS Technical Proposal, Report No. CERN/LHC/94-43 LHCC/P2, 1994 (unpublished).

[3] S. Moretti and W. J. Stirling, Phys. Lett. B **347**, 291 (1995); **366**, 451(E) (1996).

[4] A. Ballestrero, E. Maina, S. Moretti, and C. Pistarino, Phys. Lett. B **320**, 305 (1994).

[5] J. F. Gunion, H. E. Haber, F. Paige, Wu-ki Tung, and S. S. D. Willenbrock, Nucl. Phys. **B294**, 621 (1987).

[6] R. Kleiss and W. J. Stirling, Nucl. Phys. **B262**, 235 (1985).

[7] C. Mana and M. Martinez, Nucl. Phys. **B287**, 601 (1987).

[8] S. Moretti, Phys. Rev. D **50**, 2016 (1994).

[9] T. Stelzer and W. F. Long, Comput. Phys. Commun. **81**, 357 (1994).

[10] H. Murayama, I. Watanabe, and K. Hagiwara, ''HELAS: Helicity Amplitude Subroutines for Feynman Diagram Evaluations,'' KEK Report No. 91-11, 1992 (unpublished).

[11] J. A. M. Vermaseren, The Symbolic Manipulation Program FORM, Computer Algebra Netherland, Amsterdam, 1991.

[12] G. P. Lepage, J. Comput. Phys. **27**, 192 (1978).

[13] Y. Okada, M. Yamaguchi, and T. Yanagida, Prog. Theor. Phys. Lett. **85**, 1 (1991); J. Ellis, G. Ridolfi, and F. Zwirner, Phys. Lett. B **257**, 83 (1991); **262**, 477 (1991); H. E. Haber and R. Hempfling, Phys. Rev. Lett. **66**, 1815 (1991); R. Barbieri and M. Frigeni, Phys. Lett. B **258**, 395 (1991).

[14] A. Brignole, J. Ellis, G. Ridolfi, and F. Zwirner, Phys. Lett. B **271**, 123 (1991); A. Brignole, *ibid.* **277**, 313 (1992); H. E. Haber and M. A. Diaz, Phys. Rev. D **45**, 4246 (1992).

[15] V. Barger, K. Cheung, R. J. Phillips, and A. L. Stange, Phys. Rev. D **46**, 4914 (1992).

[16] W. J. Marciano, Phys. Rev. D **29**, 580 (1984).

[17] G. L. Kane, Proceedings of the ''Madison Workshop,'' 1979 (unpublished).

[18] J. H. Kühn, Acta Phys. Pol. B **12**, 347 (1981); J. H. Kühn, Acta Phys. Austriaca Suppl. **24**, 203 (1982).

[19] M. Jeżabek and J. H. Kühn, Nucl. Phys. **B320**, 20 (1989).

[20] A. D. Martin, R. G. Roberts, and W. J. Stirling, Phys. Rev. D **50**, 6734 (1994).

[21] See, for example, J. F. Gunion, H. E. Haber, G. L. Kane, and S. Dawson, *The Higgs Hunter Guide* (Addison-Wesley, Reading, MA, 1990), and references therein.

[22] A. Djouadi, J. Kalinowski, and P. M. Zerwas, Z. Phys. C **70**, 435 (1996).